Sensors & Actuators: A. Physical 368 (2024) 115101

Contents lists available at ScienceDirect

Sensors and Actuators: A. Physical

journal homepage: www.journals.elsevier.com/sensors-and-actuators-a-physical

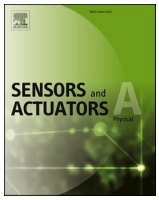

Optimization of organic field-effect transistor-based mechanical sensors to anisotropic and isotropic deformation detection for wearable and e-skin applications

Stefano Lai [a,*], Katarina Kumpf [b], Philipp Fruhmann [b], Pier Carlo Ricci [f], Johannes Bintinger [c,d], Annalisa Bonfiglio [a,e], Piero Cosseddu [a]

[a] Department of Electrical and Electronic Engineering, University of Cagliari, Piazza d'Armi, 09123 Cagliari, Italy
[b] CEST – Center for Electrochemical Surface Technology, 2700 Wr., Neustadt, Austria
[c] Biosensor Technologies, Austrian Institute of Technology, 3430 Tulln, Austria
[d] Laboratory of Organic Electronics, Department of Science and Technology, Linköping University, 601 74 Norrköping, Sweden
[e] Department of Science, Technology and Society, Scuola Universitaria Superiore IUSS, Palazzo del Broletto, Piazza della Vittoria 15, Pavia 27100, Italy
[f] Department of Physics, University of Cagliari, Complesso Universitario di Monserrato S.P. Monserrato-Sestu Km 0, 700, 09042 Monserrato, Italy

ARTICLE INFO

Keywords:
Organic transistor
Mechanical sensors
Meniscus-guided printing
Strain sensor
Bioengineering

ABSTRACT

Flexible electronics represent a viable technology for the development of innovative mechanical sensors. This paper reports a detailed study of electro-mechanical performances of Organic Field-Effect Transistor-based sensor, investigating the role of source-drain electrodes layout in combination with organic semiconductor morphology obtained by different patterning methods. Two different sensor structures, with interdigitated and spiral-shaped source and drain electrodes, are employed together with solution-processed organic semiconductors deposited by drop-casting or patterned by means of meniscus-guided printing. This technique allows the orientation of crystalline domains to specific directions, and was employed to provide anisotropic or isotropic semiconductor patterns onto the transistor's channel area. The different device configurations are tested as strain gauges and tactile sensors, by imposing anisotropic surface strain or complex deformations by means of custom-made, 3D-printed indenters. A wise choice of device structure and semiconductor patterning allows optimizing sensing performances as a response to specific deformations: interdigitated devices with crystalline domains aligned along the channel length direction are ideal strain gauges, while sensors with spiral-shaped electrodes in combination with isotropic semiconductor patterning are preferential for reproducing the sense of touch, which deals with the transduction of more complex deformation patterns. These results pave the way to the development of innovative sensors in the field of flexible bioengineering, in particular for the development of wearable and e-skin applications for joint motion monitoring and tactile sensing.

1. Introduction

Among solutions for the development of flexible electronic devices, organic materials are under the lens of the scientific community for their peculiar features, such as the intrinsic flexibility, low-temperature and solution processing with unconventional, cost-effective, large area techniques [1,2]. Flexible organic electronics has been demonstrated as a valuable technology for several applications, including the fabrication of innovative electronic circuitries [3] and, more importantly, the development of innovative sensors [4–6]. The possibility of flexible sensor development over large areas results particularly interesting in the field of mechanical deformation monitoring [7]. Most of examples in this field are related to the employment of strain sensors based on Organic Field-Effect Transistors (OFETs): by directly exploiting the transport properties of polycrystalline organic semiconductor (OSC) films, it is possible to induce mobility variation by imposing a surface strain to the transistor [8–10]. With respect to conventional mechanical sensors, such as piezoresistive strain gauges and resistive or capacitive pressure sensors, OFET-based strain sensors exploit the intrinsic advantage of transistors, such as local amplification of signals, tunable sensitivity, easier signal readout and addressing circuitries. According to the kind of stimuli applied, OFET-based strain sensors have been

* Corresponding author.
E-mail address: stefano.lai@unica.it (S. Lai).

https://doi.org/10.1016/j.sna.2024.115101
Received 30 November 2023; Received in revised form 22 January 2024; Accepted 31 January 2024
Available online 2 February 2024

effectively employed in different configurations in several bioelectronic applications. For instance, OFET-based strain gauges have been proposed to detect anisotropic deformations in joint motion monitoring [11–14]. In electronic skin (e-skin) applications, pressure sensing, which involves more complex deformation patterns, has also been explored [15–21].

Despite the fact that the above-mentioned application scenarios require the transduction of very different stimuli, a thorough investigation on the properties of OFET-based mechanical sensor structures to ensure the best functionality as strain gauges or pressure sensors is missing. Indeed, the typical OFET structure combines source and drain layout patterns defining a rectangular or an interdigitated channel with semiconductor films having randomly-directional crystalline domains, in particular when plastic substrates are involved and solution-based deposition techniques such as drop-casting are involved. As a consequence, while the source/drain layout imposes an anisotropic direction for charge transport through electrodes, the morphology of the semiconductor film is substantially isotropic, and this impede charge carriers moving along the shortest path from source to drain. This mismatch reduces the device performance both as strain gauges, where a complete anisotropic transport is fundamental to define a preferential stress direction, and as pressure sensor, where the anisotropic features of contacts reduces the natural capability of randomly-distributed crystalline domains to capture the various stress directions of a complex deformation.

Therefore, even if several examples of strain sensors based on OFETs have been reported in literature, the optimization to their performances for specific applications in mechanical sensing needs the capability of controlling both crystalline arrangement in the OSC film and the transport direction of charge carriers between electrodes. At the state-of-the-art, several techniques to promote the alignment of crystalline domains along a preferential direction have been reported as a way to improve the effective charge carrier mobility in OFETs [20–23]. These approaches can be useful for optimize OFET-based mechanical sensors as strain gauges, since the anisotropic source/drain layout would be combined with anisotropic charge carrier transport in the OSC film. Despite the technology is indeed available, a thorough electromechanical characterization of these devices to demonstrate their superior performances as strain gauges is missing. In the same way, optimized OFET-based pressure sensors (combining isotropic features in both OSC and source/drain layout) have not been explored yet.

In this paper, a systematic study on electromechanical performances of OFET-based mechanical sensors will be discussed with the aim of developing fully optimized strain gauges for anisotropic deformation detection and optimized pressure sensors, capable to effectively detect a complex deformation characterized by multiple strain directions. The proposed strategy is based on the combination of two different approaches: the meniscus-guided printing, which allows controlling crystal growth direction over significantly large areas [24,25], and the patterning of source and drain contacts with different geometrical features. In particular, together with a standard interdigitated electrode structure suitable for the development of anisotropic strain gauges, the employment of an isotropic layout for source and drain [26] will be evaluated for the development of strain sensor conceived for an effective detection of complex deformation profiles for touch and pressure sensing applications. These sensor layouts have been combined with different patterns for the organic semiconductor film and exposed to different kinds of controlled deformations in order to comprehensively characterize electromechanical performances of the devices.

2. Materials and methods

2.1. Device fabrication

OFET-based strain sensors have been fabricated using a bottom-gate, bottom-contact configuration over 50 μm-thick polyethylene terephthalate (PET) substrates, purchased from GoodFellow. The bottom gate was made by aluminum (Sigma Aldrich), thermally evaporated at a pressure of 10^{-5} Torr and further patterned by means of photolithography. The surface of the aluminum is oxidized in oven at 50 °C overnight, and then covered by a 150 nm-thick layer of Parylene C (Specialty Coating Systems), deposited by means of Chemical Vapor Deposition (CVD). Such a double dielectric layer ensures the low voltage operation of the devices [27]. Source and drain electrodes were photolithographically patterned from a thermally evaporated gold layer (Sigma Aldrich, pressure 10^{-5} Torr). Two different layouts were tested: interdigitated and spiral-shaped source and drain patterns (Fig. 1(a)). These patterns were sized to ensure the same aspect ratio W/L = 300, being W = 6 mm and L = 50 μm the channel width and length respectively. In this manuscript, devices with interdigitated and spiral-shaped electrodes will be referred as i-OFETs and s-OFETs, respectively.

2.2. Organic Semiconductor deposition and patterning

Two different approaches have been exploited for the organic semiconductor deposition (Fig. 1(b)). In order to control the crystal direction in the film, meniscus-assisted printing was employed for sensor fabrication. An EFD E2 pneumatic nozzle printer and Ultimus V pressure controller from Nordson were used in combination with a custom-made heat plate to control the temperature of the substrate. Pictures and schematics about the employed process are reported in Fig. S1 and Fig. S2 in Supplementary Information. Prior to the printing process, all equipment underwent a thorough cleaning with a combination of water and ethanol, followed by drying with a stream of nitrogen gas. The printing setup consisted of a syringe serving as the solution reservoir and a needle with a diameter of 300 μm as the printing nozzle. A solution of 6,13-Bis(triisopropylsilylethynyl)pentacene (TIPS pentacene, Sigma Aldrich) dissolved in toluene with a concentration of 15 mg/mL was used. The reservoir was connected to a Nordson Ultimus V pressure controller, allowing vacuum, forward pressure and a 3D-stage to be controlled. The printing process involved the creation of a meniscus by applying a short forward pressure pulse (typically lasting 10–20 ms at 4.48kPa). After the meniscus was formed, vacuum pressure of 0.0kPa was applied and the needle was moved across the surface at a speed of 0.5 mm/s. Throughout the process, to ensure a controlled evaporation process, a constant substrate temperature of 55 °C was maintained using the custom-made heat plate. To promote the growth of organic crystals in a specific direction, the writing speed was adjusted to match the evaporation rate of solvent at the meniscus [28]. Additionally, proper alignment of different layers during deposition was realized using a camera-based positioning system. To prevent any damage to the substrate or films, the print height was set at 130 μm. Using this technique, two different patterns were realized: i) crystal growth in parallel bands and ii) radial printing with respect to the center of the transistor. These patterns will be referred as parallel (p-) and radial (r-) patterns, respectively. Moreover, i-OFETs and s-OFETs with the organic semiconductor layer deposited by drop casting (dc-) were also fabricated. In this case, a solution of TIPS pentacene in dry anisole (10 mg/mL) was dropped onto the channel area and the solvent was evaporated at room temperature and in ambient conditions. Atomic-Force Microscopy (AFM) analysis allows evaluating that the two approaches result in semiconductor films with similar thickness (of about 100 nm, see Fig. S3 in Supplementary Information), even if in-plane crystal dimensions are significantly larger in case of drop-casting, since anisole has a boiling point higher than toluene. Nonetheless, the crystalline properties of the film are substantially similar, as derived by UV-Vis characterization of printed and drop-casted films (Fig. S4 in Supplementary Information) that highlighted typical absorption peaks of TIPS pentacene in its crystalline form (600 nm, 650 nm, 700 nm [29]).

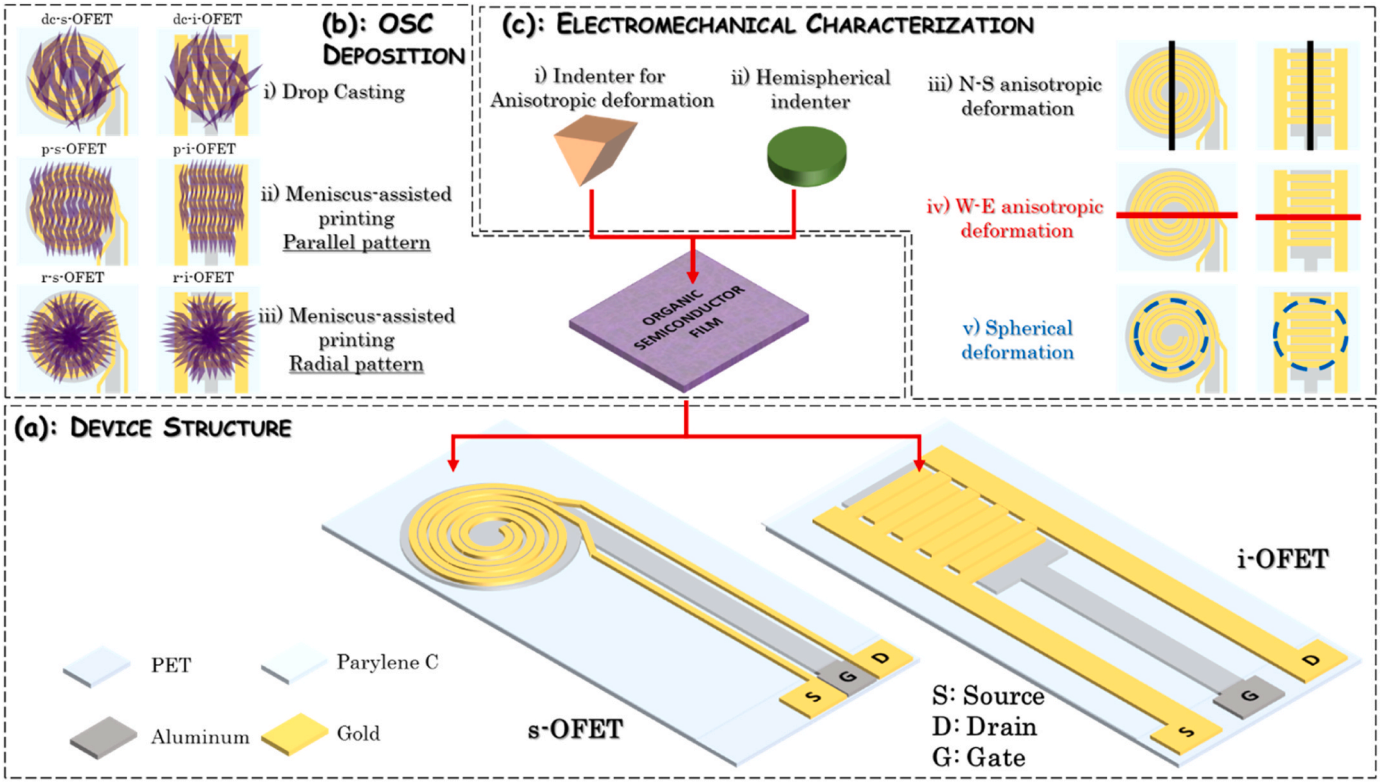

Fig. 1. (a) cartoon showing the s-OFET and i-OFET layouts; (b) different organic semiconductor patterns and deposition techniques employed; (c) kind of mechanical deformations employed during device testing as sensors.

2.3. Electrical and electromechanical characterization

Electrical characterization has been carried out in ambient conditions using a Keithley SourceMeter® 2636 with custom Matlab® software. The same system has been employed for electromechanical characterization, combined with a mechanical indenter connected to a dynamometer (Imada Digital Force Measurement Gauge). The indenter was modified with the addition of 3D-printed acrylonitrile butadiene styrene (ABS, BASF) structures to impose anisotropic and isotropic deformations (Fig. 1(c)). In particular, three different deformations have been tested: along the main axis of the device (N-S deformation), orthogonally to this direction (W-E deformation), and an isotropic one through a hemispherical intender (spherical deformation). The total width of indenters (shown in Fig. S5 in Supplementary Information) is 13 mm: the one used for anisotropic deformation is finalized with a 1.5 mm-height, triangular edge, while the radius of the hemispherical indenter is of 2 mm. The deformation was imposed on the back of the devices by controlled force values provided through the indenters. An example of real-time current vs. deformation plot is reported in Fig. S6 in Supplementary Information. Each force value was imposed ten times, and the current relative variation $\Delta I_D/I_{D0} = (I_D\text{-}I_{D0})/I_{D0}$ was evaluated at each positive edge of response. In the latter, I_D represents the current level during the application of the deformation, while I_{D0} represents the baseline current. Average and standard deviation values of applied force and corresponding current variation were then calculated.

3. Results and discussion

3.1. Device Electrical Performances

First, the electrical characterization of fabricated devices has been carried out. Table 1 reports average threshold voltage and charge carrier mobility values evaluated on a set of 5 devices for each configuration tested. Representative transfer and output characteristics are reported in Supplementary Information (Fig. S7, S8 and S9). As previously reported, [26], dc-s-OFET structures exhibit slightly higher mobilities than dc-i-OFETs thanks to charge carrier collection by spiral-shaped source and drain contacts, which turns in a larger output current in the transistor (Fig. S7). A similar result is obtained when meniscus-assisted printing is employed to pattern the organic semiconductor in the radial configuration (Fig. S8): in the case of isotropic crystalline arrangement the difference between i-OFETs and s-OFETs is more evident. In contrast, when parallel patterns are printed i-OFET configurations demonstrate superior performance compared to s-OFET (Fig. S9): this can be attributed to the alignment of crystalline domains with the channel's length, facilitating charge transport along the primary crystal axis from source to drain. It is important to note that mobility of meniscus-assisted printed devices is lower than that of drop-casted ones, as different TIPS pentacene solutions were used in the two cases. In particular, larger crystalline dimensions observed by AFM in drop-casted films, related to the higher boiling point of anisole, are the probable cause of larger mobility. It is noteworthy that solvent and concentration of solute in meniscus-assisted were chosen in order to optimize the printing performances. Nonetheless, the effect of device

Table 1
threshold voltage and charge carrier mobility in the different device structures tested. Data are reported as average ± 1-σ error bar values calculated in a set of 5 devices per each configuration.

Device Structure	OSC pattern	Threshold Voltage [Avg± 1-σ, V]	Charge Carrier Mobility [Avg± 1-σ, $cm^2V^{-1}s^{-1}$]
i-OFET	Drop-Casting	0.08 ± 0.05	$(5.3 \pm 2.2)\cdot10^{-2}$
	Radial	0.11 ± 0.07	$(2.3 \pm 1.3)\cdot10^{-2}$
	Parallel	0.01 ± 0.1	$(4.6 \pm 2)\cdot10^{-2}$
s-OFET	Drop-casting	0.08 ± 0.02	$(9.2 \pm 1.8)\cdot10^{-2}$
	Radial	0.09 ± 0.02	$(4.7 \pm 2)\cdot10^{-2}$
	Parallel	0.07 ± 0.03	$(1.3 \pm 1)\cdot10^{-2}$

geometry and patterning of organic semiconductor film is evident, as well as the improvement of device reproducibility as shown by the reduction of standard deviation among devices.

3.2. Electromechanical characterization

3.2.1. Response to anisotropic deformation

In order to characterize i-OFETs and s-OFETs with different OSC patterning as strain gauges, a triangular-shaped indenter was employed to induce a deformation on the back of the device. This deformation produces a strain along the direction of the main axis of the indenter, that can be calculated as $\varepsilon = P/S$, being P the pressure imposed by the indenter and S the Young's modulus of the device, that can be considered as the one of the PET substrate (80 MPa). On these bases, the force imposed through the dynamometer can be converted into a directional surface strain.

Calibration curves obtained for the different device configurations, subjected to a N-S anisotropic deformation, are reported in Fig. 2(a); Fig. 2(b) shows the electromechanical sensitivity, obtained as the average slope of calibration plots of two different devices per tested configuration. The behavior of i-OFETs in response to this deformation doesn't seems significantly reliant to the OSC pattern; only r-i-OFETs have a lower response, related to a slightly lower sensitivity, that can be ascribed to the lower charge carrier mobility of this particular configuration. This result is coherent with the fact that N-S deformation is applied along channel length direction, i.e. orthogonally to the preferential strain gauge deformation: therefore, no-one of the i-OFET configuration is optimized for this strain direction. For s-OFETs, the difference between meniscus-guided patterns and drop-casted OSC layer is more evident: in particular, dc-s-OFET have a sensitivity comparable to the one obtained with i-OFETs configurations, while p- and r-s-OFETs response is less than the half. This evidence is particularly interesting, since it may be expected that s-OFETs configurations are capable to intercept every anisotropic deformation direction, producing a response that may be larger than the one of i-OFETs deformed along a non-preferential direction. Nonetheless, an ideal response requires that a good matching between deformation direction, main crystalline axis orientation and source-drain transport direction is obtained. In p-s-OFETs, the deformation is applied along the main crystalline axis, thus producing the lower effect on charge transport in the semiconductor film, that combined with the low charge carrier mobility recorded in these devices justifies the worst performances with respect to p-i-OFETs. In r-s-OFETs, despite a charge carrier mobility than the one of r-i-OFETs, the number of crystalline domains aligned contemporary to the charge transport and to the deformation direction is smaller, and this explain the lower sensitivity. When the semiconductor is drop-casted, the random orientation of crystalline domains and the large charge carrier mobility contributes to improving the sensitivity.

These evidences are supported by the analysis of device response to W-E anisotropic deformation, reported in Fig. 3 in terms of calibration plots (Fig. 3(a)) and average slope on two devices per configuration (Fig. 3(b)). This deformation is applied orthogonally to the channel length direction in i-OFETs, thus being supposed to produce a larger current variation for a given strain than N-S one. Indeed, the larger response and sensitivity among all device configurations is obtained in p-i-OFETs, since this specific deformation produces a larger effect on charge transport direction, which is determined by both source-drain layout and crystalline domain alignment along channel length direction. The sensitivity almost doubles the one obtained for N-S deformation, and this suggest that p-i-OFETs are ideal candidates for the development of strain gauges with high selectivity to deformation direction. On the contrary, for all other i-OFETs configurations, the extent of the response and the sensitivity values are substantially similar to those obtained for the N-S deformation, further demonstrating that optimal performances as strain gauges require that the strain direction should be the one producing the maximum effect with respect to crystalline domains and source-drain layout at the same time. As regards s-OFETs, behavior and overall performances are similar to the one obtained for N-S deformation, with slightly larger sensitivity values recorded for meniscus-guided patterns. Summarizing the results obtained, it is possible to conclude that an OFET-based strain gauge with optimized performances requires that anisotropic features in OSC pattern and electrode layout are combined; when at least one of these is lost (due to isotropic OSC patterning or drop casting in i-OFETs, and for all s-OFET configurations), sensitivity decreases and selectivity to different deformation direction is lost.

3.2.2. Response to isotropic deformation

The response of different device configuration as tactile sensor, i.e. when an isotropic deformation is applied, is reported in Fig. 4. In this case, calibration plots (Fig. 4(a)) report relative current variation as a function of the force applied by the dynamometer through the hemispherical indenter, in a range that is compatible with tactile sensing application. Indeed, in terms of common weights, 0.2 N is roughly equivalent to the weight of a small grape or a few grains of rice, while 1.2 N is roughly equivalent to the weight of a small apple or a golf ball. Sensitivity (Fig. 4(b)) is reported as average slope of the calibration plots of two devices per configuration, thus having a N^{-1} unit measure.

For an isotropic deformation, performances of i-OFETs are substantially independent from the OSC patterning. Indeed, the hemispherical indenter is capable to induce a strain in every direction, including the preferential one for a specific configuration: along it, the device shows the maximum response, while other directions are providing a small contribution to the overall current variation. This result demonstrates that, with an anisotropic source-drain layout, the OSC patterning is less relevant on the device response to a complex deformation pattern.

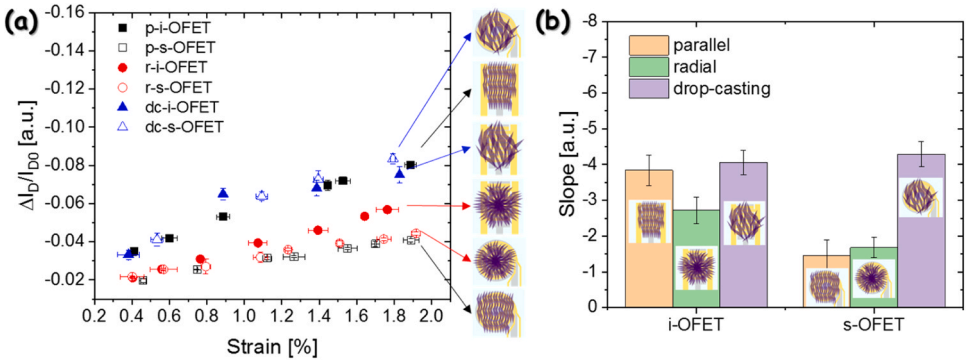

Fig. 2. (a) Calibration curves of a representative device for each configuration tested, subjected to a N-S anisotropic strain applied through the triangular-shaped indenter. Plot are reported as relative current variation vs. percentage strain. (b) Average device sensitivity, evaluated as the slope of calibration plots for two different devices per configuration tested.

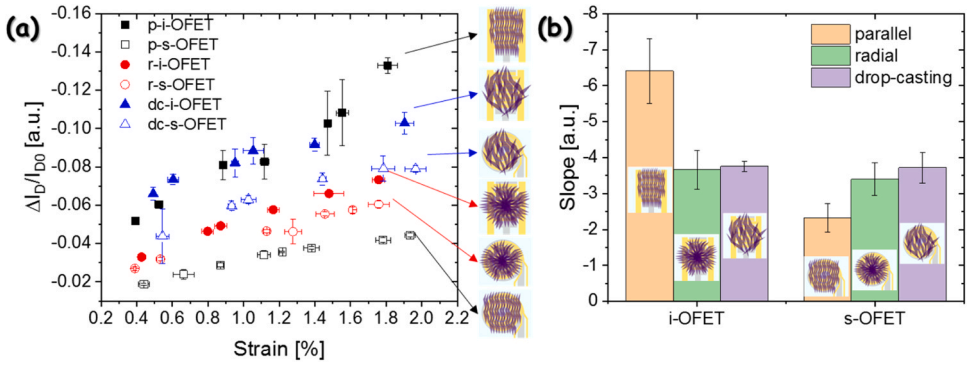

Fig. 3. (a) Calibration curves of a representative device for each configuration tested, subjected to a W-E anisotropic strain applied through the triangular-shaped indenter. Plot are reported as relative current variation vs. percentage strain. (b) Average device sensitivity, evaluated as the slope of calibration plots for two different devices per configuration tested.

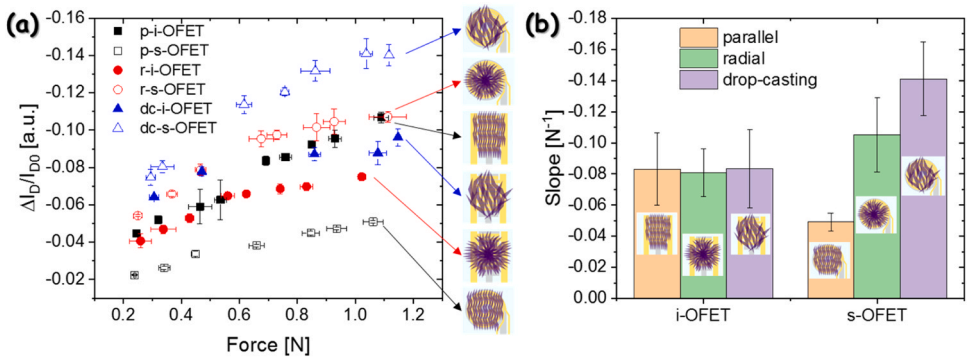

Fig. 4. (a) Calibration curves of a representative device for each configuration tested, subjected to an isotropic deformation applied through the hemispherical indenter. Plot are reported as relative current variation vs. force applied. (b) Average device sensitivity, evaluated as the slope of calibration plots for two different devices per configuration tested.

Interestingly enough, s-OFETs show a significant difference between p-, r- and dc- configurations. When the OSC patterning is anisotropic, the capability of the sensor to respond to a complex deformation is reduced since the charge transport direction is limited by the crystalline direction, even if source and drain layout is isotropic. For radial-patterned and drop-casted OSC, sensitivity increases, as the hemispherical indenter is capable to induce a deformation along the different directions in which crystals are aligned, and the spiral-shaped source and drain electrodes ensures an optimal readout of this effect in the transistor current. It is also noteworthy that the performances obtained for r-s-OFETs and dc-s-OFETs are significantly larger than the one obtained for any i-OFET configuration, further demonstrating that the capability of the device to detect its effect in crystalline domains (by ensuring an anisotropic charge carrier transport in the transistor structure) is fundamental for an optimized sensing ability of complex deformations. The better performances of dc-s-OFETs over r-s-OFETs can be justified with their larger charge carrier mobility, thus demonstrating that the optimization of OFET electrical performance is also fundamental to enhance the electromechanical response.

4. Conclusions

A comprehensive investigation of the electromechanical performance of OFET-based sensors, with a focus on understanding the impact of isotropic features in the device structure and OSC patterning was made. Two different layouts were reported in combination with meniscus-guided printing as technique for precisely controlling the crystal arrangement in the OSC film, thus enabling the optimization of charge transport directionality, either uniaxial or isotropic.

In the case of uniaxial deformation evaluation, the integration of interdigitated device structures with crystalline domains aligned along the channel length direction yielded enhanced sensitivity and superior performance in transducing deformations orthogonal to this direction, surpassing conventional drop-casting methods on similar structures or devices with isotropic features. Therefore, the need for a complete matching between crystalline alignment in the OSC film and source/drain geometry for the optimization of OFET-based mechanical sensors as strain gauges has been demonstrated.

Conversely, spiral-shaped devices with isotropic OSC patterning proved to be more effective in detecting complex deformations compared to uniaxial sensors, exhibiting superior performance relative to interdigitated devices or s-OFETs with anisotropic OSC patterning. Furthermore, the scalability and cost-effectiveness of drop-casting organic semiconductors offer a viable pathway for translating these insights into biomedical applications, particularly when combined with spiral-shaped devices.

The proposed results show that the unique attributes of flexible organic electronics enable the development and optimization of a novel class of mechanical sensors tailored to specific deformation requirements in diverse applications. This advancement holds significant promise in the realm of bioelectronics, where large-area flexible mechanical sensors can find utility in wearable devices for monitoring joint motion or gait in biomedical applications, as well as in the creation of electronic skin for prosthetic and bio-robotic applications.

CRediT authorship contribution statement

Ricci Pier Carlo: Data curation, Investigation, Validation, Writing – review & editing. **Cosseddu Piero:** Writing – original draft, Validation, Supervision, Resources, Conceptualization, Writing – review & editing.

Bonfiglio Annalisa: Writing – original draft, Supervision, Resources, Writing – review & editing. **Bintinger Johannes:** Writing – original draft, Supervision, Resources, Methodology, Funding acquisition, Conceptualization, Writing – review & editing. **Fruhmann Philipp:** Writing – original draft, Supervision, Resources, Methodology, Funding acquisition, Conceptualization, Writing – review & editing. **Kumpf Katarina:** Writing – original draft, Data curation, Conceptualization, Writing – review & editing. **Lai Stefano:** Writing – original draft, Validation, Methodology, Investigation, Formal analysis, Data curation, Conceptualization, Writing – review & editing.

Declaration of Competing Interest

The authors declare that they have no known competing financial interests or personal relationships that could have appeared to influence the work reported in this paper.

Data Availability

Data will be made available on request.

Acknowledgments

P.F. and J. B. gratefully acknowledge the Gesellschaft für Forschungsförderung NÖ (GFF) for funding this work under grant-No.: LSC19-013, and the Österreichische Forschungsförderungs GmbH (FFG) for funding the Centre of Electrochemical Surface Technology within the COMET program (grant-No.: 865864).

Appendix A. Supporting information

Supplementary data associated with this article can be found in the online version at doi:10.1016/j.sna.2024.115101.

References

[1] L. Li, L. Han, H. Hu, R. Zhang, A review on polymers and their composites for flexible electronics, Mater. Adv. 4 (2023) 726–746, https://doi.org/10.1039/D2MA00940D.
[2] H. Liu, D. Liu, J. Yang, H. Gao, Y. Wu, Flexible electronics based on organic semiconductors: from patterned assembly to integrated applications, Small 19 (2023) 2206938, https://doi.org/10.1002/smll.202206938.
[3] H. Matsui, Y. Takeda, S. Tokito, Flexible and printed organic transistors: from materials to integrated circuits, Org. Electron. 75 (2019) 105432, https://doi.org/10.1016/j.orgel.2019.105432.
[4] X. Zhang, Z. Pu, X. Su, C. Li, H. Zheng, D. Li, Flexible organic field-effect transistors-based biosensors: progress and perspectives, Anal. Bioanal. Chem. 415 (2023) 1607–1625, https://doi.org/10.1007/s00216-023-04553-6.
[5] S. Li, W. Tang, S. Chen, Y. Si, R. Liu, X. Guo, Flexible organic polymer gas sensor and system integration for smart packaging, Adv. Sens. Res. (2023) 2300030, https://doi.org/10.1002/adsr.202300030.
[6] Z. Wang, G. Shen, Flexible optoelectronic sensors: status and prospects, Mater. Chem. Front. 7 (2023) 1496–1519, https://doi.org/10.1039/D2QM01319C.
[7] Z.A. Lamport, M.R. Cavallari, K.A. Kam, C.K. McGinn, C. Yu, I. Kymissis, Organic thin film transistors in mechanical sensors, Adv. Funct. Mater. 30 (2020) 2004700, https://doi.org/10.1002/adfm.202004700.
[8] P. Cosseddu, S. Milita, A. Bonfiglio, Strain sensitivity and transport properties in organic field-effect transistors, IEEE Electron Dev. Lett. 33 (2012) 113–115, https://doi.org/10.1109/LED.2011.2173898.
[9] P. Cosseddu, G. Tiddia, S. Milita, A. Bonfiglio, Continuous tuning of the mechanical sensitivity of Pentacene OTFTs on flexible substrates: from strain sensors to deformable transistors, Org. Electron. 14 (2013) 206–211, https://doi.org/10.1016/j.orgel.2012.10.033.
[10] V. Scenev, P. Cosseddu, A. Bonfiglio, I. Salzmann, N. Severin, M. Oehzelt, N. Koch, J.P. Rabe, Origin of mechanical strain sensitivity of pentacene thin-film transistors, Org. Electron. 14 (2013) 1323–1329, https://doi.org/10.1016/j.orgel.2013.02.030.
[11] S.H. Nam, P.J. Jeon, S.W. Min, Y.T. Lee, E.Y. Park, S. Im, Highly sensitive non-classical strain gauge using organic heptazole thin-film transistor circuit on a flexible substrate, Adv. Funct. Mater. 24 (2014) 4413–4419, https://doi.org/10.1002/adfm.201400139.
[12] T.Q. Trung, N.T. Tien, D. Kim, M. Jang, O.J. Yoon, N.-E. Lee, A flexible reduced graphene oxide field-effect transistor for ultrasensitive strain sensing, Adv. Funct. Mater. 24 (2014) 117–124, https://doi.org/10.1002/adfm.201301845.
[13] Z.W. Wang, S.J. Guo, H.W. Li, B. Wang, Y.T. Sun, Z.Y. Xu, X.S. Chen, K.J. Wu, X. T. Zhang, F.F. Xing, L.Q. Li, W.P. Hu, The semiconductor/conductor interface piezoresistive effect in an organic transistor for highly sensitive pressure sensors, Adv. Mater. 31 (2019) 1805630, https://doi.org/10.1002/adma.201805630.
[14] S. Lai, A. Garufi, F. Madeddu, G. Angius, A. Bonfiglio, P. Cosseddu, A wearable platform for monitoring wrist flexion and extension in biomedical applications using organic transistor-based strain sensors, IEEE Sens. J. 19 (2019) 6020–6028, https://doi.org/10.1109/JSEN.2019.2909174.
[15] D.-I. Kim, T.Q. Trung, B.-U. Hwang, J.-S. Kim, S. Jeon, J. Bae, J.-J. Park, N.-E. Lee, A sensor array using multi-functional field-effect transistors with ultrahigh sensitivity and precision for bio-monitoring, Sci. Rep. 5 (2015) 12705, https://doi.org/10.1038/srep12705.
[16] R.A. Nawrocki, N. Matsuhisa, T. Yokota, T. Someya, 300-nm imperceptible, ultraflexible, and biocompatible e-skin fit with tactile sensors and organic transistors, Adv. Electron. Mater. 2 (2016) 1500452, https://doi.org/10.1002/aelm.201500452.
[17] S.O. Yeo, S. Park, T.J. Yi, D.H. Kim, J.A. Lim, Highly sensitive flexible pressure sensors based on printed organic transistors with centro-apically self-organized organic semiconductor microstructures, ACS Appl. Mater. Interfaces 9 (2017) 42996–43003, https://doi.org/10.1021/acsami.7b15960.
[18] Y.P. Zang, H.G. Shen, D.Z. Huang, X.-A. Di, D.B. Zhu, A dual-organic-transistor-based tactile-perception system with signal-processing functionality, Adv. Mater. 29 (2017) 1606088, https://doi.org/10.1002/adma.201606088.
[19] F.A. Viola, A. Spanu, P.C. Ricci, A. Bonfiglio, P. Cosseddu, Ultrathin, flexible and multimodal tactile sensors based on organic field-effect transistors, Sci. Rep. 8 (2018) 8073, https://doi.org/10.1038/s41598-018-26263-1.
[20] X. Wang, W. Lu, P. Wei, Z. Qin, N. Qiao, X. Qin, M. Zhang, Y. Zhu, L. Bu, G. Lu, Artificial tactile recognition enabled by flexible low-voltage organic transistors and low-power synaptic electronics, ACS Appl. Mater. Interfaces 14 (2022) 48948–48959, https://doi.org/10.1021/acsami.2c14625.
[21] E. Karner-Petritz, A. Petritz, T. Uemura, N. Namba, T. Araki, T. Sekitani, B. Stadlober, Ultraflexible organic active matrix sensor sheet for tactile and biosignal monitoring, Adv. Electron. Mater. (2023) 2201333, https://doi.org/10.1002/aelm.202201333.
[22] Y. Diao, L. Shaw, Z. Bao, S.C.B. Mannsfeld, Morphology control strategies for solution-processed organic semiconductor thin films, Energy Environ. Sci. 7 (2014) 2145–2159, https://doi.org/10.1039/C4EE00688G.
[23] Z. Wu, Y. Yan, Y. Zhao, Y. Liu, Recent advances in realizing highly aligned organic semiconductors by solution-processing approaches, Small Methods 6 (2022) 2200752, https://doi.org/10.1002/smtd.202200752.
[24] C. Ren, L. Cao, T. Wu, Meniscus-guided deposition of organic semiconductor thin films: materials, mechanism, and application in organic field-effect transistors, Small 19 (2023) 2300151, https://doi.org/10.1002/smll.202300151.
[25] S. Yang, S. Park, J. Bintinger, Y. Bonnassieux, J. Anthony, I. Kymissis, Employing pneumatic nozzle printing for controlling the crystal growth of small molecule organic semiconductor for field-effect transistors, Adv. Electron. Mater. 4 (2018) 1700534, https://doi.org/10.1002/aelm.201700534.
[26] S. Lai, K. Kumpf, P.C. Ricci, P. Fruhmann, J. Bintinger, A. Bonfiglio, P. Cosseddu, Isotropic contact patterning to improve reproducibility in organic thin-film transistors, Org. Electron. 122 (2023) 106887, https://doi.org/10.1016/j.orgel.2023.106887.
[27] P. Cosseddu, S. Lai, M. Barbaro, A. Bonfiglio, Ultra-low voltage, organic thin film transistors fabricated on plastic substrates by a highly reproducible process, Appl. Phys. Lett. 100 (2012) 093305, https://doi.org/10.1063/1.3691181.
[28] S. Yang, S. Park, J. Bintinger, Y. Bonnassieux, I. Kymissis, P-99: pneumatic nozzle printing as a versatile approach to crystal growth management and patterning of printed organic thin film transistors, SID Symp. . Dig. Tech. Pap. 47 (2016) 1502–1505, https://doi.org/10.1002/sdtp.10983.
[29] D.A. Kadri, D.A. Karim, M. Seck, K. Diouma, M. Pasquinelli, Optimization of 6, 13Bis (triisopropylsilylethynyl) pentacene (TIPS-Pentacene) organic field effect transistor: annealing temperature and solvent effects, Mater. Sci. Appl. 9 (2018) 900–912, https://doi.org/10.4236/msa.2018.911065.

Stefano Lai obtained *magna cum laude* the M.Sc. Degree in Electronics in 2010. He joined the Department of Electrical and Electronic Engineering as Ph.D. student in 2011. He received the Ph.D. in Electronics and Computer Science in 2014. Since 2021, he is a Senior Assistant Professor in Bioengineering. His research interests involve the development, fabrication and characterization of innovative organic flexible electronics applications, related in particular to the employment of organic thin-film transistors for sensing in biomedical and soft-robotics applications.

Katarina Kumpf studied Electronics at the University of Applied Science Technikum Wien and Biomedical Engineering at the Technical University of Vienna for her master's degrees. In 2019, she joined the Center for Electrochemical Surface Technology (CEST) as a junior researcher, focusing on the reproducible production of chemiresistors based on conducting polymers, as well as their implementation in Internet of Things applications In 2022, she joined the Medical University of Vienna, where she is working in the field of data science.

Philipp Fruhmann completed his Ph.D. studies in Technical Chemistry at the Vienna University of Technology in 2013. He continued his research as postdoctoral fellow at the Institute of Applied Synthetic Chemistry until 2015, when he joined the Center for Electrochemical Surface Technology (CEST). Since then, he is working as Senior Researcher in the field of (bio-)sensors with focus on linking strategies, molecularly imprinted and conductive polymers, and the design of organic surfaces.

Johannes Bintinger obtained his PhD in Technical Chemistry at the Vienna University of Technology in 2016, then joined the Center for Electrochemical Surface Technology (CEST) and in 2017 the Austrian Institute of Technology to work on electronic gas- and biosensors (co-founder of NOSI), before joining the Linköping University in 2019 where he is working on iontronic drug delivery systems (ERC) and conductive polymers (CEO of n-ink).

Annalisa Bonfiglio graduated in Physics at the University of Genova in 1991 and got the PhD in Bioengineering at the Politechnical School in Milan in 1996. She currently holds a joint position of Full Professor of Electronic Bioengineering at the University of Cagliari and at the Scuola Universitaria Superiore IUSS of Pavia. She authored more than 200 papers on international journals, conference proceedings, book chapters. She also holds 12 patents. Her research activity is focussed on innovative materials and devices for wearable electronics and biomonitoring.

Piero Cosseddu obtained his Ph.D. in Electronic and Computer Science Engineering in 2007 at the University of Cagliari. He is currently Associate Professor in the Department of Electrical and Electronics Engineering of the University of Cagliari, Italy. His research activity has been mainly focused on the field of Organic Electronics with particular attention towards the design, fabrication and characterization of organic semiconductor-based devices on flexible plastic substrates, and their application for the development of innovative sensing systems for different application areas, such bio-chemical sensors, wearable electronics and artificial skin.